



HAL
open science

Molecular-level investigation into UV-induced transformation of hydrophobic aquatic dissolved organic matter

Suona Zhang, Zhineng Hao, Jingfu Liu, Jean-Philippe Croué

► **To cite this version:**

Suona Zhang, Zhineng Hao, Jingfu Liu, Jean-Philippe Croué. Molecular-level investigation into UV-induced transformation of hydrophobic aquatic dissolved organic matter. *Science of the Total Environment*, 2022, 842, pp.156959. 10.1016/j.scitotenv.2022.156959 . hal-04433726

HAL Id: hal-04433726

<https://hal.science/hal-04433726v1>

Submitted on 22 Jul 2024

HAL is a multi-disciplinary open access archive for the deposit and dissemination of scientific research documents, whether they are published or not. The documents may come from teaching and research institutions in France or abroad, or from public or private research centers.

L'archive ouverte pluridisciplinaire **HAL**, est destinée au dépôt et à la diffusion de documents scientifiques de niveau recherche, publiés ou non, émanant des établissements d'enseignement et de recherche français ou étrangers, des laboratoires publics ou privés.



Distributed under a Creative Commons Attribution - NonCommercial 4.0 International License

1
2 **Molecular-level Investigation into UV-induced Transformation of**
3 **Hydrophobic Aquatic Dissolved Organic Matter**
4

5
6
7
8 Suona Zhang,^{†,§} Zhineng Hao,[§] Jingfu Liu,[§] and Jean-Philippe Croue^{*,†,‡}
9

10
11
12 [†]Curtin Water Quality Research Centre, Department of Chemistry, Curtin University, Perth
13 6102, Australia

14 [§]Research Center for Eco-Environmental Sciences, Chinese Academy of Sciences, Beijing
15 10085, China

16 [‡]Institut de Chimie des Milieux et des Matériaux IC2MP UMR 7285 CNRS, Université de
17 Poitiers, Poitiers 86000, France
18

19
20
21 Corresponding author:

22 *jean.philippe.croue@univ-poitiers.fr; Tel.: +33 (0) 7 87 09 44 66
23

24

Abstract

25 The ubiquitously present dissolved organic matter (DOM) greatly influence the efficiency of
26 UV-based technologies due to its reactivity to UV irradiation. In this work, UV-induced
27 changes within three hydrophobic DOM fractions isolated from different surface waters were
28 investigated. Analysis on UV absorbance at 254 nm, electron donating capacity, fluorescence
29 intensity and carbon content revealed small changes in DOM bulk properties associated with
30 the UV-induced photochemical reactions. Fourier transform ion cyclotron resonance mass
31 spectrometry (FT-ICR MS) was further used to explore the modification of the molecular
32 distribution based on H/C and O/C ratios, m/z and DBE. The molecular-level investigation
33 revealed that an average of 296 aromatic and lignin-like molecules were degraded, leading to
34 the production of around 306 new molecules. The UV-reactive community were identified as
35 CHO molecules with higher DBE (>10) and carbon number (>25) which could be readily
36 transformed into smaller saturated molecules. Molecules containing nitrogen(N) or sulfur(S)
37 atom, independent of aromaticity and molecular weight (m/z), were also highly UV
38 susceptible and transformed into molecules with larger DBE and m/z . Possible reaction
39 pathways responsible for the observations were discussed. The results indicated that UV-
40 reactivity and subsequent transformation of DOM are remarkably correlated with its
41 molecular composition and characteristics. Though the changes in bulk properties of DOM
42 following UV irradiation were observed to be very small, the significant alteration in its
43 molecular structures would have a profound impact on the UV-based treatment processes.

44 **Keywords:** UV irradiation; aquatic DOM; FT-ICR MS; reactive molecules; transformation.

45

46 **1. Introduction**

47 The strong efficiency of UV-based technologies, UV or UV-based advanced oxidation
48 processes (UV-AOPs), for disinfection or removal of emerging contaminants is well
49 documented (Ji et al. 2018, Li and Blatchley III 2009, Qin et al. 2019, Sharpless and Linden
50 2003, Zhang et al. 2017). It is also known that dissolved organic matter (DOM) greatly
51 influence the efficiency of the UV-based processes. Due to the prevalence of chromophoric
52 structures, DOM can readily absorb and interact with UV light, leading to a complex
53 sequence of direct and indirect photolysis reactions. This may hinder the efficiency of UV-
54 based technologies due to light attenuation, but contrariwise, generate reactive species
55 through DOM photosensitization which can contribute to the elimination of organic
56 contaminants (Berg et al. 2019, Serna-Galvis et al. 2017). UV-induced DOM reactivity would
57 directly define the efficacy of a UV-based process and impact the downstream water quality,
58 e.g., through formation of disinfection by-products, microbial regrowth nutrients, etc
59 (Imoberdorf and Mohseni 2011, Magnuson et al. 2002, Thomson et al. 2002a). For instance,
60 UV-irradiated DOM was reported to be more reactive to chlorine, leading to an increase in
61 the formation of disinfection byproducts (Magnuson et al. 2002, Meng et al. 2016). UV
62 exposure can also alter the bioavailability of DOM to microorganisms and consequently the
63 efficiency of the biological treatment (Sulzberger and Durisch-Kaiser 2009, Thomson et al.
64 2002b). UV irradiation may also induce toxicity following DOM transformation (Frimmel
65 1998, He et al. 2015). Therefore, it is crucial to elucidate the UV-induced alteration of DOM
66 to provide fundamental knowledge and better understanding on the reactivity of irradiated
67 DOM.

68 Previous study has documented insignificant changes of DOM in optical properties and size
69 distribution under various UV doses (i.e., up 140 mJ·cm⁻²) typical for disinfection (Magnuson
70 et al. 2002). Interestingly, another study reported an increase in UV absorbance of DOM with

71 similar UV doses ($\sim 60 \text{ mJ}\cdot\text{cm}^{-2}$) (Meng et al. 2016). Elevated UV dosages ($10^4\text{--}10^5 \text{ mJ}\cdot\text{cm}^{-2}$)
72 can lead to the depletion of chromophoric structures, transformation of higher molecular
73 weight (MW) hydrophobic (HPO) fractions to hydrophilic counterparts with lower MW, and
74 even carbon removal (Buchanan et al. 2005, Corin et al. 1996). However, the ultimate
75 molecular-level information shaping the reactivity and influencing the transformation of
76 DOM bulk properties during UV irradiation was not yet provided.

77 Electrospray ionization Fourier transform ion cyclotron resonance mass spectrometry (FT-
78 ICR MS) has been widely used for the molecular-level investigation of DOM transformation
79 in various UV-based (e.g., UV/H₂O₂, UV/persulfate and UV/Chlorine) as well as other (e.g.,
80 ozonation and chlorination) engineered processes (Andersson et al. 2020, Phungsai et al.
81 2016, 2018, 2019, Ruan et al. 2021, Zhang et al. 2021). Due to the ultrahigh resolution and
82 accuracy of this novel technique, molecules for individual mass peak could be
83 unambiguously assigned, and the corresponding molecular characteristics and the changes
84 could be easily obtained. For instance in DOM matrix, molecules with higher aromaticity and
85 MW were found more reactive in UV/H₂O₂ or UV/PDS process, and transformed into
86 molecules with lower aromatic character and MW (Zhang et al. 2021). The analytic tool has
87 remarkable potential in providing detailed information on the UV-induced transformation of
88 DOM at a molecular-level. The application of this advanced technique in photochemical
89 transformation of DOM in natural aquatic systems has also been widely documented
90 (Gonsior et al. 2009, Mesfioui et al. 2015, Miranda et al. 2020, Stubbins et al. 2010, Wilske
91 et al. 2020). Numerous molecular-level observations have been obtained in respective system
92 with the use of natural sunlight or light sources simulating sunlight. However, the use of 254
93 nm light as irradiation source, widely used in water treatment processes, remains missing
94 among these previous work. Considering the highly heterogeneous character of DOM, the
95 shift to shorter wavelength/higher energy irradiation would cause the response/reaction of

96 different compositions and the formation of different products. The information plays a
97 crucial role in better application of UV-based water treatment strategies and improvement of
98 water quality.

99 To fill these knowledge gaps, 254 nm UV-induced changes in DOM were investigated with
100 the characterization of both bulk properties using traditional analytic tools (e.g., UV-vis
101 spectrophotometer and fluorometer) and molecular characteristics using FT-ICR MS. The
102 pool of molecules reactive to and produced from UV (i.e., 254 nm) irradiation was identified.
103 The possible UV-triggered reaction pathways were putatively presented based on the
104 comparison between UV-reactive and UV-produced molecules. Humic substances (i.e., HPO
105 DOM fractions) isolated from three surface waters and presenting different aromatic
106 character (i.e., SUVA value) were used in this investigation.

107 **2. Experimental Section**

108 **2.1 Chemicals and DOM samples.**

109 High-performance liquid chromatography (HPLC) grade methanol (MeOH) and ethyl acetate
110 (EtOAc) were supplied by Honeywell Burdick & Jackson. Sulfuric acid (H₂SO₄, 98%) and
111 hydrochloric acid (HCl, 32%) were purchased from UNIVAR. (3-ethylbenzothiazoline-6-
112 sulfonic acid) diammonium salt (ABTS; ≥98%) was provided by Sigma-Aldrich. Three
113 surface water DOM fractions previously isolated were selected for investigation:
114 Hydrophobic acids isolated from Suwannee River water (S-HPOA, USA), hydrophobic DOM
115 from Ribou Reservoir (R-HPO, France), and hydrophobic DOM from Colorado River (C-
116 HPO, USA). The basic characteristics of the DOM samples have been reported in previous
117 studies (Niu et al. 2018, Zhang et al. 2021). Briefly, S-HPOA exhibited a highest SUVA
118 value (aromaticity) of 4.93, a medium SUVA (3.16) recorded with R-HPO, and the lowest
119 SUVA (2.01) for C-HPO.

120 **2.2 Experimental procedures.**

121 A low pressure (LP)-UV collimated beam device (CBD) was used for UV irradiation
122 experiments. Briefly, the CBD is equipped with a total of three 15 W low-pressure Hg UV-
123 lamps. A xy-cross slide table with a magnetic stirrer was employed to accommodate the UV
124 reactor. An incident UV-C intensity of $\sim 0.9 \text{ mW}\cdot\text{cm}^{-2}$ determined using a certified UV-C
125 radiometer was applied to irradiate a 250 mL DOM solution ($\sim 4 \text{ mgC}\cdot\text{L}^{-1}$) in a petri-dish
126 (i.e., UV reactor, 84 mm in diameter). The initial UV fluence was further corrected with
127 radiometer, divergence, reflection, petri and water factor (Bolton and Linden 2003). UV
128 doses of 633, 760, and 886 $\text{mJ}\cdot\text{cm}^{-2}$ were calculated for S-HPOA-, R-HPO-, and C-HPO-
129 containing solutions, respectively. Experiments were performed in absence of buffer to avoid
130 the potential formation of buffer-derived radicals. System pH dropped from ~ 4.74 to ~ 3.21
131 after 30 min irradiation. Samples for FT-ICR MS analysis were acidified to $\sim \text{pH } 2$ and then
132 extracted by solid phase extraction (SPE) using Bond Elut PPL cartridges (6 mL, 1 g, Agilent
133 Technologies). The extraction procedure was previously reported for FT-ICR MS analysis
134 (Zhang et al. 2021).

135 **2.3 Analytic methods**

136 **2.3.1 Analysis of bulk properties**

137 Bulk DOM properties were analysed using a Cary 60 spectrophotometer for UV_{254}
138 measurement (Agilent, USA), a Shimadzu TOC-L analyser (SHIDMAZU, Japan) for TOC
139 (Total Organic Carbon) determination, and a fluorescence spectrometer (Cary Eclipse, Varian)
140 for FEEM (Fluorescence Excitation Emission Matrix) recording (Zhang et al. 2019). The
141 analysis of EDC (Electron Donating Capacity) of DOM samples using size exclusion
142 chromatography (SEC) based on the method developed by Chon et al. (2015). Briefly, DOM
143 sample was injected into A TOYOPEARL HW-50S column (8 mm \times 30 cm) using 50 mM
144 borate eluent at a flow rate of 0.2 mL/min. Following separation, post-column reaction of

145 DOM with the oxidant ABTS^{•+} took place in a reaction coil. ABTS^{•+} was generated through
146 oxidation of ABTS by sodium persulfate under acidic conditions and injected to the reaction
147 coil at 0.05 mL/min using a helium pressurised generator. Finally, two UV detectors (Agilent
148 1100 series, USA) positioned in series were used for recording UV absorbance of DOM at
149 254 nm and the signal for ABTS/ABTS^{•+} at 405 nm.

150 2.3.2 FT-ICR MS analysis

151 Procedures of sample pre-treatment by SPE using Bond Elut PPL cartridges (6 mL, 1 g,
152 Agilent Technologies) (Dittmar et al. 2008) and sample analysis using 15.0 T Bruker Solarix
153 FT-ICR MS were detailed in our previous publication (Zhang et al. 2021). Information on
154 molecular assignment, classification of molecules based on H/C and O/C, and calculation of
155 molecular characteristics can also be found in this article (Zhang et al. 2021).

156 3. Results and discussion

157 3.1 UV-induced changes in bulk properties of DOM

158 Upon 30 min UV irradiation with an incident intensity of $\sim 0.9 \text{ mW}\cdot\text{cm}^{-2}$, a slight decrease in
159 UV_{254} of the DOM samples was observed. Specifically, the decrease was recorded as 3%, 3%,
160 and 11% for S-HPOA, R-HPO, and C-HPO (Fig. 1a), respectively. It was more pronounced
161 with C-HPO, finding attributed to its lower initial UV_{254} value, leading to a lower calculated
162 water factor and greater UV fluence. The change in EDC with UV irradiation was also
163 observed and found comparable with that of UV_{254} except for S-HPOA (Fig. 1a). The
164 nominally higher decrease in EDC (i.e., 6%) than UV_{254} (i.e., 3%) for S-HPOA was probably
165 related with its initial higher content of phenolic structures (i.e., major EDC contributors)
166 (Zhang et al. 2019). A greater UV_{254} decrease compared to EDC was previously interpreted
167 as a reaction initiated with hydroxyl radical addition to non-phenolic aromatic rings, the
168 opposite was considered to refer to an initiated depletion of phenolic moieties with the
169 preservation of aromatic structures (Chon et al. 2015, Zhang et al. 2019). The findings in the

170 current study implied that a UV-specific reaction mechanism was involved in the
171 transformation of DOM.

172 **Fig. 1.**

173 Changes of fluorescence properties following the irradiation of DOM solutions was also
174 investigated based on the modifications recorded in the EEM spectra, i.e., excitation (Ex) and
175 emission (Em) maxima. Two fluorescent peaks denoted as Peak I and Peak II (Fig. 1b and Fig.
176 S1) typical of hydrophobic fractions were detected. A decrease in peak intensity was
177 determined for R-HPO (e.g., approximately 13% for Peak II) and C-HPO (e.g.,
178 approximately 43% for Peak II), indicating the transformation of fluorescent structures to less
179 or non-fluorescent components. Interestingly, an increase in the intensity of both peaks (~
180 45%) were observed for S-HPOA (Table S1). The enhancement in fluorescence signal after
181 UV irradiation or radical-based oxidation processes has also been reported (Meng et al. 2016,
182 Zhang et al. 2019). Moreover, not only was a change in the fluorescence intensity observed
183 before and after UV irradiation, but also a shift of the EEM spectra peak. For instance, the
184 emission wavelength of peak II shifted from 456 nm to 450 nm, 438 to 430 nm and 448 to
185 440 nm (Table S1) for S-HPOA, R-HOP, and C-HPO, respectively. The blue shift of the
186 emission wavelength implied the formation of smaller fluorescent molecules (Korshin et al.
187 1999) probably due to UV-induced bond cleavage. The more significant variation in
188 fluorescence as compared to that of UV₂₅₄ indicated a more pronounced UV-induced
189 transformation of fluorescent chromophores than non-fluorescent components. In addition, no
190 significant change in DOC concentration was observed for all DOM samples subjected to UV
191 irradiation. The results reflected that UV-induced changes in molecular compositions and
192 characteristics occurred without carbon mineralization under current experimental conditions.

193 **3.2 UV-induced molecular changes of DOM**

194 The numbers of assigned molecules before and after UV irradiation were 1974/1990,
195 2886/2838, and 2513/2578 for S-HPOA, R-HPO, and C-HPO, respectively. Parameters such
196 as DBE, modified aromaticity index (AImod), m/z , H/C, O/C, and nominal oxidation state of
197 carbon (NOSC) (Koch and Dittmar 2006, LaRowe and Van Cappellen 2011, Remucal et al.
198 2020, Yuan et al. 2017) widely used to reflect specific DOM properties (i.e., degree of
199 unsaturation, molecular size, and degree of oxygenation), were calculated. Based on the
200 molecular-level statistics of the assigned peaks (Table S2), some differences in the molecular
201 characteristics of the three DOM isolates were observed. Specifically, S-HPOA showed
202 highest DBE and m/z (i.e., averaged value for all the assigned molecules), but the lowest level
203 of nitrogen (N) or sulfur (S) incorporation (0.16%) and NOSC (-0.18). R-HPO exhibited
204 medium DBE but the highest N or S content (0.45%) and NOSC (0.05). The smallest DBE
205 was determined for C-HPO which also exhibited medium level of N or S elements (0.19%)
206 and NOSC (-0.10). A van Krevelen diagram was plotted to visualize the distribution of the
207 detected molecules based on their H/C and O/C as well as relative peak intensity (i.e., as
208 represented by the bubble size, Fig. 2). Generally, no pronounced difference in the molecular
209 distribution (i.e., due to the minimal change in H/C or O/C) was found between the original
210 and the irradiated samples for the three DOM isolates (Fig. 2). Interestingly, the appearance
211 of N- or S- containing molecules with even lower H/C and O/C after UV irradiation were
212 found in all three DOM samples. This finding is different from what was previously detected
213 in radical-based oxidation processes, where an increase in saturation and oxidation state was
214 observed (Zhang et al. 2021). Furthermore, the change in the calculated H/C or O/C of the
215 DOM samples before and after irradiation was also negligible (Table S2). The observed
216 molecular-level changes in H/C or O/C was probably due to the incomplete UV-specific
217 reactions as discussed in the following sections.

218

Fig. 2.

219 3.3 UV-reactive, stable and produced molecules

220 Based on previous studies (Remucal et al. 2020, Yuan et al. 2017), the disappeared molecules
221 (i.e., the molecular formulas detected in the original samples but not in the irradiated samples)
222 were considered as UV-reactive, while the appeared molecules (i.e., molecular formulas
223 detected only in the irradiated samples but not in the original samples) were denoted as UV-
224 produced. Approximately 200–350 molecules disappeared upon UV irradiation, accounting
225 for only 10%–14% of the molecules in original samples (Table 1). Around 200–400 new
226 molecules appeared after UV exposure, contributing to 10–16% of the pool of molecules in
227 the treated samples (Table 1). The cumulative intensity of disappeared or appeared molecules
228 represented only few per cents of the overall peak intensity detected for the initial or treated
229 samples (Table 1), indicating that these molecule species were less abundant or efficient in
230 generating signal. The van Krevelen plot (Fig. 3) showed the distributions of three sets of
231 molecules, i.e., disappeared, remained and appeared, based on their H/C and O/C. The
232 disappeared molecules primarily showed H/C and O/C indicative of aromatic or phenolic
233 structures (i.e., H/C = 0.7–1.5, O/C = 0.1–0.67, Fig. 3). Considering the semi-quantitative
234 nature of peak intensity, intensity-weighted average values of molecular characteristics such
235 as H/C_{wa} , O/C_{wa} , and DBE_{wa} for the disappeared, appeared and remained molecules were
236 calculated and summarized in Table 1. Interestingly, lower H/C_{wa} (~5%) and O/C_{wa} (~6%)
237 were detected for disappeared molecules as compared to the remained structures (Table 1).
238 Furthermore, the disappeared molecules showed remarkably larger m/z_{wa} (~17%) and DBE_{wa}
239 (~23%) than the remained ones (Table 1), indicating the preferential UV targeting of
240 molecules with larger size and greater unsaturation. In addition, molecules incorporating N or
241 S were more UV-labile than the counterparts containing only CHO, as indicated by the higher
242 relative abundance of these molecules within the pool of disappeared molecules (Fig. 3 and
243 Table 1). Interestingly, exposure to UV led to the formation of molecules with lower H or O

244 content (Table 1), as described by the decreased H/C_{wa} (~7%) and O/C_{wa} (~15%). For the
245 remained pool, molecules with change in peak intensity before and after irradiation, may also
246 contribute to the UV-reactive and UV-produced pool. Previous studies (Jennings et al. 2022,
247 Phungsai et al. 2016, 2019) have applied 30% or 50% intensity change as cut-off line for the
248 identification of these molecules from the remained pool. We also calculated the relative
249 intensity change of each molecule, based on which a van Krevelen diagram for the remained
250 molecules was plotted (Fig. S2). As shown in Fig. S2, the intensity variation for the majority
251 of the molecules is within 20%. Molecules showing 30% decrease or increase in intensity
252 only accounted for less than 6% of the remained pool for the three DOM fractions, and the
253 percentages for those with 50% variation is even lower. Due to the small number of these
254 molecules and the comparison uncertainty, the contribution of the remained molecules to the
255 reactive or the produced pool was not quantitatively discussed in drawing conclusions.
256 However, molecules with 30% change in intensity was taken into account to support some of
257 our conclusions.

258 **Fig. 3.**

259 **Table 1.**

260 **3.3.1 UV-reactive molecules**

261 To examine the role of unsaturation, molecular size as well as non-oxygen heteroatoms in
262 UV susceptibility, the disappeared and the remained molecules were plotted based on their
263 DBE and C number. For the disappeared pool, significantly different distribution in the DBE
264 versus C number map was observed between sole CHO and non-oxygen heteroatom
265 containing molecules (i.e., CHON, CHOS, and CHONS) (Fig. S3). For instance, the majority
266 of the disappeared CHO molecules occupied a region with larger DBE as well as C number,
267 while CHON, CHOS, and CHONS molecules mainly distributed in a region with smaller
268 DBE and C number. Based on this observation, the following discussion was conducted by

269 categorizing the molecules into two subgroups, i.e., molecules containing only CHO and also
270 N or S (denoted as CHO+N/S). The UV-reactive CHO molecules showed larger DBE as well
271 as C number (Fig. 4), for instance, the disappeared molecules were primary those with a
272 DBE >10 and a C number >25. Interestingly, the reactive CHO+N/S molecules spanned the
273 same range of DBE and C carbon as the preserved counterparts (Fig. 4). The potentially UV-
274 reactive molecules in the remained pool (i.e., with intensity decrease >30%) was also
275 estimated regarding their aromaticity and molecular size, and identical observations with the
276 disappeared molecules were obtained (Fig. S4). For instance, 108 out of 110 such molecules
277 in S-HOPA contained only CHO and exhibited larger DBE and C number (Fig. S4a), and 38
278 out of 53 such molecules belonging to CHO+N/S subgroup in R-HPO primarily distributed in
279 the region with smaller DBE and C number (Fig. S4b). The results indicated that CHO
280 molecules with higher degree of unsaturation as well as complexity were more UV sensitive.
281 However, the reactivity of the molecules bearing non-oxygen heteroatoms was independent
282 of molecular unsaturation and size. Though larger MW molecules were reported more
283 reactive to UV exposure, this observation provided complementary information for the
284 identification of UV reactive molecules. Moreover, the different observations regarding UV
285 reactivity for the CHO and CHO+N/S molecules implied disparate UV-induced reactions
286 between the two subgroups.

287 **Fig. 4.**

288 **3.3.2 UV-produced molecules**

289 **3.3.2.1 Shift in carbon number**

290 Exposure to UV irradiation caused the appearance of 208, 307 and 405 molecules following
291 the disappearance of 192, 355 and 340 molecules for S-HPOA, R-HPO, and C-HPO,
292 respectively. To characterize the UV-induced molecular-level transformation of DOM, the
293 number of produced molecules and reactive (i.e., disappeared) molecules were plotted as a

294 function of carbon number (Fig. 5) and DBE (Fig. 6) and presented separately as two
295 subgroups (i.e., CHO and CHO+N/S molecules). Different trends in the shift of carbon
296 number were observed between CHO and CHO+N/S molecules for the three DOM isolates
297 (Fig. 5). For CHO subgroup, the respective number of removed/produced molecules for S-
298 HPOA, R-HPO, and C-HPO was 170/145, 122/134, and 122/148. Generally, a shift in C
299 number from larger to smaller upon UV irradiation could be detected, with the specific range
300 of C number varying for different DOM samples (Fig. 5a, c, and e). For instance, a
301 remarkable decrease in number (i.e., from 115 to 50) was observed with molecules bearing
302 30–38 carbons for the produced molecules as compared to the reactive ones, primarily
303 followed by a number increase (~62%) of molecules with <30 C atoms in S-HPOA (Fig. 5a).
304 Interestingly, an increase of compounds with larger C number (~40) was also observed for
305 the three DOM samples (Fig. 5a, c, and e), which will be explained in Section 3.4. For the
306 CHO+N/S subgroup, the removed/produced number pair was 22/63, 233/173, and 218/257
307 for S-HPOA, R-HPO, and C-HPO, respectively. Specifically, the increased CHO+N/S
308 molecules in S-HPOA were found incorporating more carbon atoms (14–30), with the
309 disappearance of the smaller molecules (i.e., with a carbon number lower than 11) upon UV
310 irradiation. The lost CHO+N/S molecules observed with R-HPO were mainly those with a
311 carbon number ranging from 15–30. Interestingly, the loss of C-HPO CHO+N/S molecules
312 with a carbon number between 17 and 23 was followed by the formation of molecules with
313 even higher carbon number (24–32).

314 Fig. 5.

315 3.3.2.2 Shift in DBE

316 For the CHO subgroup, a significant decrease in the number was found with molecules
317 showing a DBE >12 for all the DOM isolates, mainly accompanied by an increase of
318 molecules with lower DBE (Fig. 6). A different trend in the change of DBE was observed

319 with CHO+N/S subgroup. For S-HPOA, the newly formed molecules were found with larger
320 DBE (i.e., >7) than the disappeared molecules. A remarkable loss of molecules with DBE
321 ranging from 7 to 14 was observed with R-HPO, followed by the formation of molecules with
322 DBE <7 or >14. Interestingly, the major depletion of molecules for C-HPO occurred with
323 those showing DBE between 9 and 13, also leading to the formation of molecules with
324 greater DBE. The observed converse trend between CHO and CHO+N/S subgroups clearly
325 indicated that the characterization on bulk properties could not fully reflect the changes at a
326 molecular level and the nature of the transformation.

327 As reflected by the yellow bar in Fig. 5 and 6, the potentially UV-reactive molecules (i.e.,
328 with intensity decrease greater than 30% in the remained pool) also exhibited the same trend
329 in the shift of carbon number. For instance, the vast majority of such molecules in S-HPOA
330 belong to the CHO subgroup, and they were featured with larger C number and DBE as also
331 observed with the disappeared molecules. For R-HPO, the potentially UV-reactive molecules
332 were primarily in the CHO+N/S subgroup, and their C number and DBE also fell into the
333 same range observed with the disappeared molecules. The consistency in the molecule
334 aromaticity and size between the UV-reactive and potentially UV-reactive molecules, further
335 confirms the conclusions drawn in this work by only comparing disappeared and appeared
336 molecules. However, limitation of the current conclusions remains due to the uncertainty in
337 identifying reactive and produced molecules.

338 **Fig. 6.**

339 **3.4 Putative UV-induced reaction pathways responsible for the observed changes**

340 The reactivity of DOM to UV irradiation is highly dependent on its molecular composition
341 and characteristics. The presence of non-oxygen heteroatoms, unsaturation level, and
342 molecular size played an important role in shaping DOM reactivity. CHO molecules with

343 higher molecular weight (i.e., C number >25) and degree of unsaturation (i.e., DBE >10)
344 were more UV reactive. The reaction would readily be initiated through photon absorption by
345 these electron-rich complex structures, leading to the degradation of the molecules (Helms et
346 al. 2014, Sarathy and Mohseni 2007, Schmitt-Kopplin et al. 1998, Sulzberger and Durisch-
347 Kaiser 2009). These electron-rich complex moieties of CHO molecules seem to undergo only
348 partial depletion as indicated by the insignificant shift in C number and DBE (Table S2, Fig.
349 5 and 6) as well as H/C_{wa} and O/C_{wa} (Table S2, Fig S5 and S6). The minor changes could
350 probably be attributed to the weak photoreactions mainly inducing cleavage between
351 aromatic structures (Scheme 1a). It should be noted that Photo-Fries rearrangement (Scheme
352 1b) could also occur, which however could not be detected due to the formation of
353 isomerization products (Coppinger and Bell 1966, Griesser et al. 2009). The larger molecules
354 (i.e., as indicated by the emergence of molecules with larger C numbers in Fig. 5a, c and e)
355 could probably be the products of UV-induced breakdown of specific molecules unable to be
356 detected in the original samples. There is also a possibility that they were produced through
357 the UV-induced covalent linking of benzophenone to target molecules (Scheme 1c)
358 (Hermanson 2013, Ross et al. 2003). This distinct UV-induced photo-process involving
359 primary photoproducts (e.g., radical cations, electrons and triplets) and reactive intermediates
360 (e.g., ¹O₂, O₂^{•-}, and •OH) is different from that of a radical-dominant (e.g., •OH) system. This
361 hypothesis is supported by the different UV₂₅₄ and EDC decrease relationship (Fig. 1) as the
362 one reported in radical-based oxidation system (Zhang et al. 2021). As a consequence,
363 distinct reaction pathways as well as products would be expected in a UV-induced DOM
364 transformation.

365 The reactivity of CHO+N/S molecules showed no dependency on unsaturation level and
366 molecular size. Remarkably, molecules with even more carbons and DBE were found upon
367 UV irradiation (Fig. 5 and 6), probably through either breakdown of originally undetected

368 molecules or covalent linkage between molecules (Zhong et al. 2001). For the latter, larger
369 molecules could probably be produced through the transformation of triazole-containing or
370 alike structures (Eicher et al. 2013, Kahle et al. 2008) under 254 nm UV irradiation. For
371 instance, benzotriazole has been widely used and detected in aquatic systems due to its
372 resistance to biodegradation (Giger et al. 2006, Osburn et al. 2016). The structures thus
373 present in aquatic DOM could undergo alkylation (Scheme 1d) or polymerisation (Scheme 1e)
374 upon UV treatment, leading to formation of bigger molecules and loss of N elements (Liu et
375 al. 2011). The release of N₂ due to bond scission of N-N in these reactions (Scheme 1d and e)
376 could be supported by the decrease of nitrogen content after UV irradiation (10–30%, Table
377 S2). The co-functioning of the chromophoric CHO and CHO+N/S molecules may explain the
378 small changes in its optical properties. The UV-induced transformation may have profound
379 impact on the water quality (e.g., toxicity) (Frimmel 1998, He et al. 2015) and subsequent
380 water treatment process (e.g, disinfection, membrane filtration and biological treatment)
381 (Sulzberger and Durisch-Kaiser 2009, Thomson et al. 2002b).

Scheme 1.

4. Conclusions

384 Small but significant 254 nm UV-induced changes were observed with three HPO DOM
385 isolates exhibiting different level of aromaticity and non-oxygen heteroatom incorporation.
386 Though minor changes in bulk properties such as EDC, UV₂₅₄, fluorescence intensity or
387 carbon content were measured, remarkable transformation of UV-reactive components
388 occurred at a molecular-level. The UV-reactive CHO molecules were characterized with
389 larger C number (i.e, >25) and DBE (i.e, >10), consequently transformed into smaller
390 saturated components. Independent of aromaticity and complexity, molecules containing N or
391 S were also UV-reactive. Formation of larger molecules were found with these molecules
392 probably through UV-induced covalent linkage.

393 The results of the current study also revealed that the initial composition and characteristics
394 of DOM played a significant role in shaping its reactivity toward UV irradiation. The
395 difference in the reactivity would lead to distinct transformation products and consequently
396 influence on the UV-based treatment process or water quality. The findings provided new
397 insights into the application of UV-based technology especially the direct UV treatment
398 technique. However, the results found in this study may not be expected in a typical UV
399 disinfection process as the dosages applied (600–900 mJ·cm⁻²) were higher than that for UV
400 disinfection (40–100 mJ·cm⁻²).

401 **Acknowledgments**

402 The authors acknowledge the PhD scholarship provided by China Scholarship Council and
403 Curtin University to Suona Zhang.

404 **Reference**

- 405 Andersson, A., Lavonen, E., Harir, M., Gonsior, M., Hertkorn, N., Schmitt-Kopplin, P., Kylin,
406 H. and Bastviken, D. (2020) Selective removal of natural organic matter during drinking
407 water production changes the composition of disinfection by-products. *Environmental*
408 *Science: Water Research & Technology* 6(3), 779-794.
- 409 Berg, S.M., Whiting, Q.T., Herrli, J.A., Winkels, R., Wammer, K.H. and Remucal, C.K.
410 (2019) The role of dissolved organic matter composition in determining photochemical
411 reactivity at the molecular level. *Environmental Science & Technology* 53(20), 11725-11734.
- 412 Bolton, J.R. and Linden, K.G. (2003) Standardization of Methods for Fluence (UV Dose)
413 Determination in Bench-Scale UV Experiments. *Journal of Environmental Engineering*
414 129(3), 209-215.
- 415 Buchanan, W., Roddick, F., Porter, N. and Drikas, M. (2005) Fractionation of UV and VUV
416 Pretreated Natural Organic Matter from Drinking Water. *Environmental Science &*
417 *Technology* 39(12), 4647-4654.

- 418 Chon, K., Salhi, E. and von Gunten, U. (2015) Combination of UV absorbance and electron
419 donating capacity to assess degradation of micropollutants and formation of bromate during
420 ozonation of wastewater effluents. *Water Research* 81, 388-397.
- 421 Coppinger, G.M. and Bell, E.R. (1966) Photo-Fries Rearrangement of Aromatic Esters. Role
422 of Steric and Electronic Factors. *The Journal of Physical Chemistry* 70(11), 3479-3489.
- 423 Corin, N., Backlund, P. and Kulovaara, M. (1996) Degradation products formed during UV-
424 irradiation of humic waters. *Chemosphere* 33(2), 245-255.
- 425 Dittmar, T., Koch, B., Hertkorn, N. and Kattner, G. (2008) A simple and efficient method for
426 the solid-phase extraction of dissolved organic matter (SPE-DOM) from seawater.
427 *Limnology and Oceanography: Methods* 6(6), 230-235.
- 428 Eicher, T., Hauptmann, S. and Speicher, A. (2013) *The chemistry of heterocycles: structures,*
429 *reactions, synthesis, and applications*, John Wiley & Sons.
- 430 Frimmel, F.H. (1998) Impact of light on the properties of aquatic natural organic matter.
431 *Environment International* 24(5), 559-571.
- 432 Giger, W., Schaffner, C. and Kohler, H.-P.E. (2006) Benzotriazole and Tolyltriazole as
433 Aquatic Contaminants. 1. Input and Occurrence in Rivers and Lakes. *Environmental Science*
434 *& Technology* 40(23), 7186-7192.
- 435 Gonsior, M., Peake, B.M., Cooper, W.T., Podgorski, D., D' Andrilli, J. and Cooper, W.J.
436 (2009) Photochemically Induced Changes in Dissolved Organic Matter Identified by
437 Ultrahigh Resolution Fourier Transform Ion Cyclotron Resonance Mass Spectrometry.
438 *Environmental Science & Technology* 43(3), 698-703.
- 439 Griesser, T., Höfler, T., Jakopic, G., Belzik, M., Kern, W. and Trimmel, G. (2009) Refractive
440 index modulation in polymers bearing photoreactive phenyl and naphthyl ester units using
441 different UV wavelengths. *Journal of Materials Chemistry* 19(26), 4557-4565.
- 442 He, X., de la Cruz, A.A., Hiskia, A., Kaloudis, T., O'Shea, K. and Dionysiou, D.D. (2015)
443 Destruction of microcystins (cyanotoxins) by UV-254 nm-based direct photolysis and
444 advanced oxidation processes (AOPs): Influence of variable amino acids on the degradation
445 kinetics and reaction mechanisms. *Water Research* 74, 227-238.
- 446 Helms, J.R., Mao, J., Stubbins, A., Schmidt-Rohr, K., Spencer, R.G.M., Hernes, P.J. and
447 Mopper, K. (2014) Loss of optical and molecular indicators of terrigenous dissolved organic
448 matter during long-term photobleaching. *Aquatic Sciences* 76(3), 353-373.
- 449 Hermanson, G.T. (2013) *Bioconjugate Techniques (Third Edition)*. Hermanson, G.T. (ed), pp.
450 229-258, Academic Press, Boston.

- 451 Imoberdorf, G. and Mohseni, M. (2011) Degradation of natural organic matter in surface
452 water using vacuum-UV irradiation. *Journal of Hazardous Materials* 186(1), 240-246.
- 453 Jennings, E., Kremser, A., Han, L., Reemtsma, T. and Lechtenfeld, O.J. (2022) Discovery of
454 Polar Ozonation Byproducts via Direct Injection of Effluent Organic Matter with Online LC-
455 FT-ICR-MS. *Environmental Science & Technology* 56(3), 1894-1904.
- 456 Ji, Y., Yang, Y., Zhou, L., Wang, L., Lu, J., Ferronato, C. and Chovelon, J.-M. (2018)
457 Photodegradation of sulfasalazine and its human metabolites in water by UV and
458 UV/peroxydisulfate processes. *Water Research* 133, 299-309.
- 459 Kahle, M., Buerge, I.J., Hauser, A., Müller, M.D. and Poiger, T. (2008) Azole Fungicides:
460 Occurrence and Fate in Wastewater and Surface Waters. *Environmental Science &*
461 *Technology* 42(19), 7193-7200.
- 462 Koch, B.P. and Dittmar, T. (2006) From mass to structure: an aromaticity index for high-
463 resolution mass data of natural organic matter. *Rapid Communications in Mass Spectrometry*
464 20(5), 926-932.
- 465 Korshin, G.V., Kumke, M.U., Li, C.-W. and Frimmel, F.H. (1999) Influence of chlorination
466 on chromophores and fluorophores in humic substances. *Environmental Science &*
467 *Technology* 33(8), 1207-1212.
- 468 LaRowe, D.E. and Van Cappellen, P. (2011) Degradation of natural organic matter: A
469 thermodynamic analysis. *Geochimica et Cosmochimica Acta* 75(8), 2030-2042.
- 470 Li, J. and Blatchley III, E.R. (2009) UV Photodegradation of Inorganic Chloramines.
471 *Environmental Science & Technology* 43(1), 60-65.
- 472 Liu, Y.-S., Ying, G.-G., Shareef, A. and Kookana, R.S. (2011) Photolysis of benzotriazole
473 and formation of its polymerised photoproducts in aqueous solutions under UV irradiation.
474 *Environmental Chemistry* 8(2), 174-181.
- 475 Magnuson, M.L., Kelty, C.A., Sharpless, C.M., Linden, K.G., Fromme, W., Metz, D.H. and
476 Kashinkunti, R. (2002) Effect of UV Irradiation on Organic Matter Extracted from Treated
477 Ohio River Water Studied through the Use of Electrospray Mass Spectrometry.
478 *Environmental Science & Technology* 36(23), 5252-5260.
- 479 Meng, Y., Wang, Y., Han, Q., Xue, N., Sun, Y., Gao, B. and Li, Q. (2016) Trihalomethane
480 (THM) formation from synergic disinfection of biologically treated municipal wastewater:
481 Effect of ultraviolet (UV) irradiation and titanium dioxide photocatalysis on dissolve organic
482 matter fractions. *Chemical Engineering Journal* 303, 252-260.

- 483 Mesfioui, R., Abdulla, H.A.N. and Hatcher, P.G. (2015) Photochemical Alterations of
484 Natural and Anthropogenic Dissolved Organic Nitrogen in the York River. *Environmental*
485 *Science & Technology* 49(1), 159-167.
- 486 Miranda, M.L., Osterholz, H., Giebel, H.A., Bruhnke, P., Dittmar, T. and Zielinski, O. (2020)
487 Impact of UV radiation on DOM transformation on molecular level using FT-ICR-MS and
488 PARAFAC. *Spectrochimica Acta Part A: Molecular and Biomolecular Spectroscopy* 230,
489 118027.
- 490 Niu, X.-Z., Harir, M., Schmitt-Kopplin, P. and Croué, J.-P. (2018) Characterisation of
491 dissolved organic matter using Fourier-transform ion cyclotron resonance mass spectrometry:
492 Type-specific unique signatures and implications for reactivity. *Science of The Total*
493 *Environment* 644, 68-76.
- 494 Osburn, C.L., Handsel, L.T., Peierls, B.L. and Paerl, H.W. (2016) Predicting Sources of
495 Dissolved Organic Nitrogen to an Estuary from an Agro-Urban Coastal Watershed.
496 *Environmental Science & Technology* 50(16), 8473-8484.
- 497 Phungsai, P., Kurisu, F., Kasuga, I. and Furumai, H. (2016) Molecular characterization of
498 low molecular weight dissolved organic matter in water reclamation processes using Orbitrap
499 mass spectrometry. *Water Research* 100, 526-536.
- 500 Phungsai, P., Kurisu, F., Kasuga, I. and Furumai, H. (2018) Changes in dissolved organic
501 matter composition and disinfection byproduct precursors in advanced drinking water
502 treatment processes. *Environmental Science & Technology* 52(6), 3392-3401.
- 503 Phungsai, P., Kurisu, F., Kasuga, I. and Furumai, H. (2019) Molecular characteristics of
504 dissolved organic matter transformed by O₃ and O₃/H₂O₂ treatments and the effects on
505 formation of unknown disinfection by-products. *Water Research* 159, 214-222.
- 506 Qin, R., How, Z.T. and Gamal El-Din, M. (2019) Photodegradation of naphthenic acids
507 induced by natural photosensitizer in oil sands process water. *Water Research* 164, 114913.
- 508 Remucal, C.K., Salhi, E., Walpen, N. and von Gunten, U. (2020) Molecular-Level
509 Transformation of Dissolved Organic Matter during Oxidation by Ozone and Hydroxyl
510 Radical. *Environmental Science & Technology* 54(16), 10351-10360.
- 511 Ross, G.F., Smith, P.M., McGregor, A., Turnbull, D.M. and Lightowers, R.N. (2003)
512 Synthesis of Trifunctional PNA–Benzophenone Derivatives for Mitochondrial Targeting,
513 Selective DNA Binding, and Photo-Cross-Linking. *Bioconjugate Chemistry* 14(5), 962-966.
- 514 Ruan, X., Xiang, Y., Shang, C., Cheng, S., Liu, J., Hao, Z. and Yang, X. (2021) Molecular
515 characterization of transformation and halogenation of natural organic matter during the

- 516 UV/chlorine AOP using FT-ICR mass spectrometry. *Journal of Environmental Sciences* 102,
517 24-36.
- 518 Sarathy, S.R. and Mohseni, M. (2007) The Impact of UV/H₂O₂ Advanced Oxidation on
519 Molecular Size Distribution of Chromophoric Natural Organic Matter. *Environmental*
520 *Science & Technology* 41(24), 8315-8320.
- 521 Schmitt-Kopplin, P., Hertkorn, N., Schulten, H.-R. and Kettrup, A. (1998) Structural changes
522 in a dissolved soil humic acid during photochemical degradation processes under O₂ and N₂
523 atmosphere. *Environmental Science & Technology* 32(17), 2531-2541.
- 524 Serna-Galvis, E.A., Ferraro, F., Silva-Agrede, J. and Torres-Palma, R.A. (2017) Degradation
525 of highly consumed fluoroquinolones, penicillins and cephalosporins in distilled water and
526 simulated hospital wastewater by UV₂₅₄ and UV₂₅₄/persulfate processes. *Water Research* 122,
527 128-138.
- 528 Sharpless, C.M. and Linden, K.G. (2003) Experimental and Model Comparisons of Low- and
529 Medium-Pressure Hg Lamps for the Direct and H₂O₂ Assisted UV Photodegradation of N-
530 Nitrosodimethylamine in Simulated Drinking Water. *Environmental Science & Technology*
531 37(9), 1933-1940.
- 532 Stubbins, A., Spencer, R.G.M., Chen, H., Hatcher, P.G., Mopper, K., Hernes, P.J., Mwamba,
533 V.L., Mangangu, A.M., Wabakanghanzi, J.N. and Six, J. (2010) Illuminated darkness:
534 Molecular signatures of Congo River dissolved organic matter and its photochemical
535 alteration as revealed by ultrahigh precision mass spectrometry. *Limnology and*
536 *Oceanography* 55(4), 1467-1477.
- 537 Sulzberger, B. and Durisch-Kaiser, E. (2009) Chemical characterization of dissolved organic
538 matter (DOM): a prerequisite for understanding UV-induced changes of DOM absorption
539 properties and bioavailability. *Aquatic Sciences* 71(2), 104-126.
- 540 Thomson, J., Roddick, F. and Drikas, M. (2002a) Natural organic matter removal by
541 enhanced photo-oxidation using low pressure mercury vapour lamps. *Water Supply* 2(5-6),
542 435-443.
- 543 Thomson, J., Roddick, F. and Drikas, M. (2002b) UV photooxidation facilitating biological
544 treatment for the removal of NOM from drinking water. *Journal of Water Supply: Research*
545 *and Technology—AQUA* 51(6), 297-306.
- 546 Wilske, C., Herzsprung, P., Lechtenfeld, O.J., Kamjunke, N. and von Tuempling, W. (2020)
547 Photochemically induced changes of dissolved organic matter in a humic-rich and forested
548 stream. *Water* 12(2), 331.

- 549 Yuan, Z., He, C., Shi, Q., Xu, C., Li, Z., Wang, C., Zhao, H. and Ni, J. (2017) Molecular
550 Insights into the Transformation of Dissolved Organic Matter in Landfill Leachate
551 Concentrate during Biodegradation and Coagulation Processes Using ESI FT-ICR MS.
552 *Environmental Science & Technology* 51(14), 8110-8118.
- 553 Zhang, S., Hao, Z., Liu, J., Gutierrez, L. and Croué, J.-P. (2021) Molecular insights into the
554 reactivity of aquatic natural organic matter towards hydroxyl ($\cdot\text{OH}$) and sulfate ($\text{SO}_4^{\cdot-}$)
555 radicals using FT-ICR MS. *Chemical Engineering Journal* 425, 130622.
- 556 Zhang, S., Rouge, V., Gutierrez, L. and Croue, J.-P. (2019) Reactivity of chromophoric
557 dissolved organic matter (CDOM) to sulfate radicals: Reaction kinetics and structural
558 transformation. *Water Research* 163, 114846.
- 559 Zhang, Y., Zhang, J., Xiao, Y., Chang, V.W.C. and Lim, T.-T. (2017) Direct and indirect
560 photodegradation pathways of cytostatic drugs under UV germicidal irradiation: Process
561 kinetics and influences of water matrix species and oxidant dosing. *Journal of Hazardous*
562 *Materials* 324, 481-488.
- 563 Zhong, H., Wang, J., Jia, X., Li, Y., Qin, Y., Chen, J., Zhao, X.S., Cao, W., Li, M. and Wei,
564 Y. (2001) Fabrication of Covalently Attached Ultrathin Films Based on Dendrimers via H-
565 Bonding Attraction and Subsequent UV Irradiation. *Macromolecular Rapid Communications*
566 22(8), 583-586.
- 567

568 **Figure Captions**

569 **Fig. 1.** Changes in (a) UV₂₅₄ and EDC of the three DOM isolates and (b) FEEM of R-HPO
570 arising from 30 min UV irradiation. Conditions: Incident UV intensity = 0.9 mW·cm⁻²,
571 [TOC]₀ = 3.89 ± 0.18 mgC·L⁻¹, at unadjusted pH (4.74 ± 0.19) and room temperature (20 °C).

572 **Fig. 2.** van Krevelen diagrams of the DOM isolates before and after UV irradiation (30 min).
573 Bubble size reflects the relative peak intensity of the assigned molecules.

574 **Fig. 3.** van Krevelen diagrams (left) and relative abundance of molecules with different
575 compositions (right) for the disappeared, remained and produced molecules upon 30 min UV
576 irradiation.

577 **Fig. 4.** DBE versus C number map showing distribution of disappeared and remained
578 molecules containing (a,c,e) only CHO and (b,d,f) also N or S. Bubble size reflects the
579 relative abundance of the molecules (i.e., the number of the molecules).

580 **Fig. 5.** Number of molecules associated with Carbon number within disappeared, remained
581 and produced (a,c,e) CHO and (b,d,f) CHO+N/S community upon 30 min UV irradiation.
582 Note: The remained molecules are only those with intensity decrease greater than 30%.

583 **Fig. 6.** Number of molecules associated with DBE within disappeared, remained and
584 produced (a,c,e) CHO and (b,d,f) CHO+N/S community upon 30 min UV irradiation. Note:
585 The remained molecules are only those with intensity decrease greater than 30%.

586 **Scheme 1.** Representative illustrations on UV-induced reactions responsible for the observed
587 DOM transformation. (a). Cleavage of large DOM molecules (b). Photo-Fries rearrangement
588 of phenyl ester (c) Covalent linkages between benzophenone and target molecules. (d)
589 Addition of alkyl to benzotriazole structures (e) Polymerization of benzotriazole structures.
590 R-H represents active H-containing target molecules.

591

592

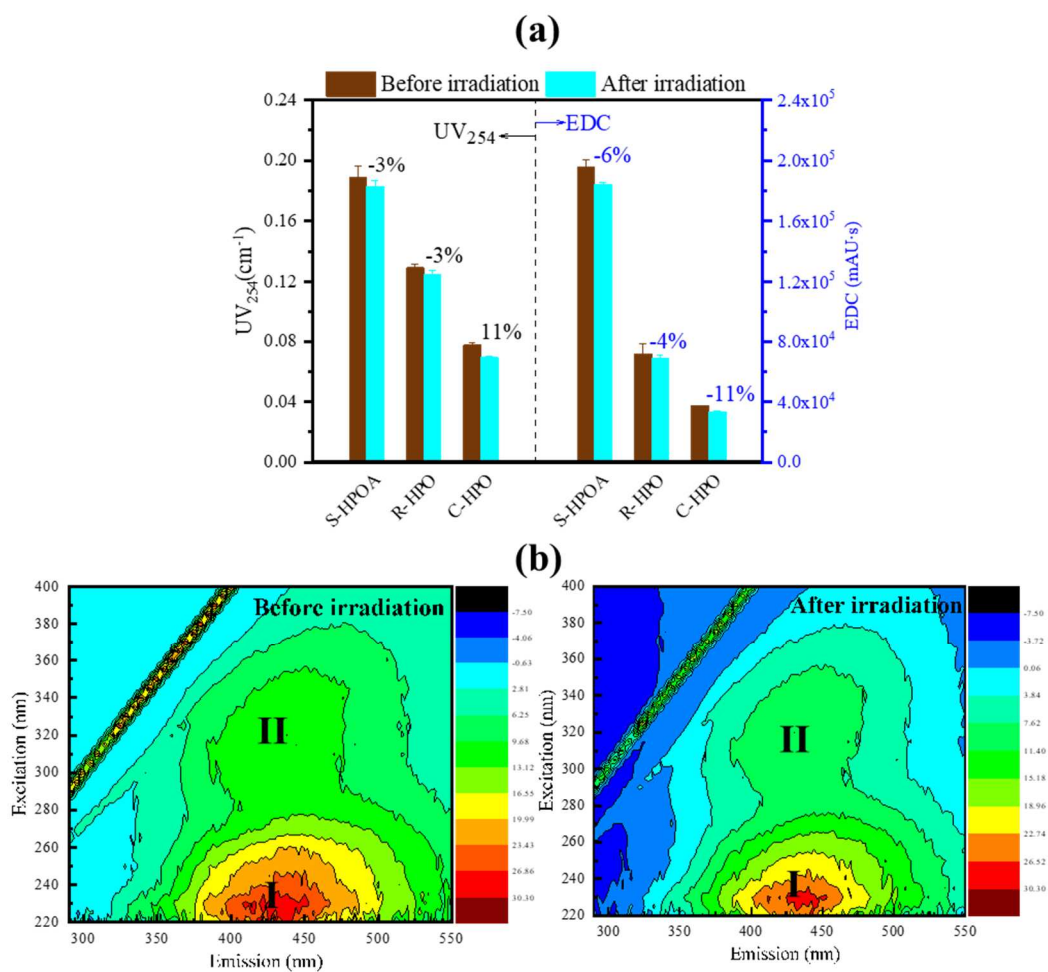


Fig. 1. Changes in (a) UV₂₅₄ and EDC of the three DOM isolates and (b) FEEM of R-HPO arising from 30 min UV irradiation. Conditions: Incident UV intensity = 0.9 mW·cm⁻², [TOC]₀ = 3.89 ± 0.18 mgC·L⁻¹, at unadjusted pH (4.74 ± 0.19) and room temperature (20 °C).

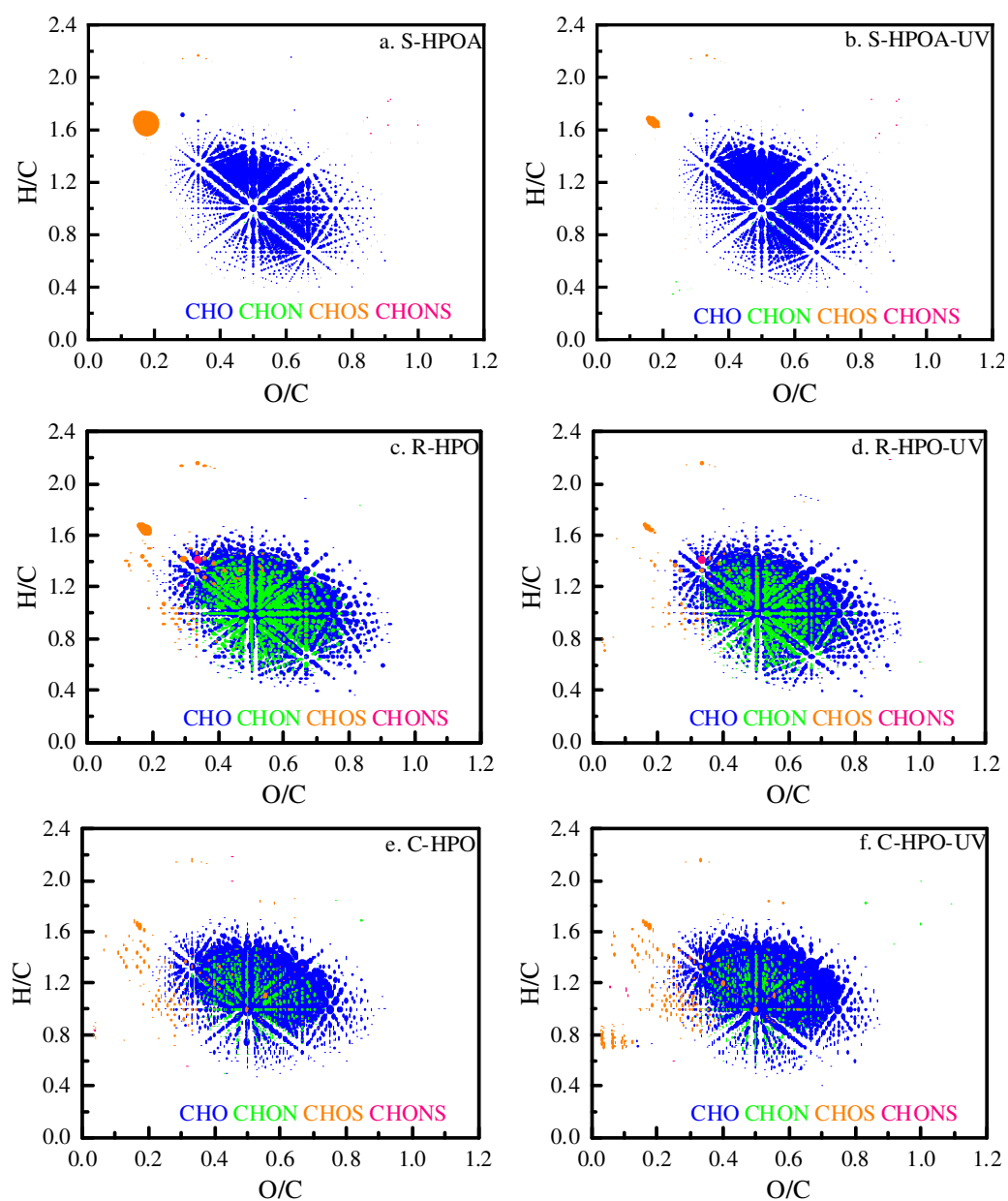


Fig. 2. van Krevelen diagrams of the DOM isolates before and after UV irradiation (30 min). Bubble size reflects the relative peak intensity of the assigned molecules.

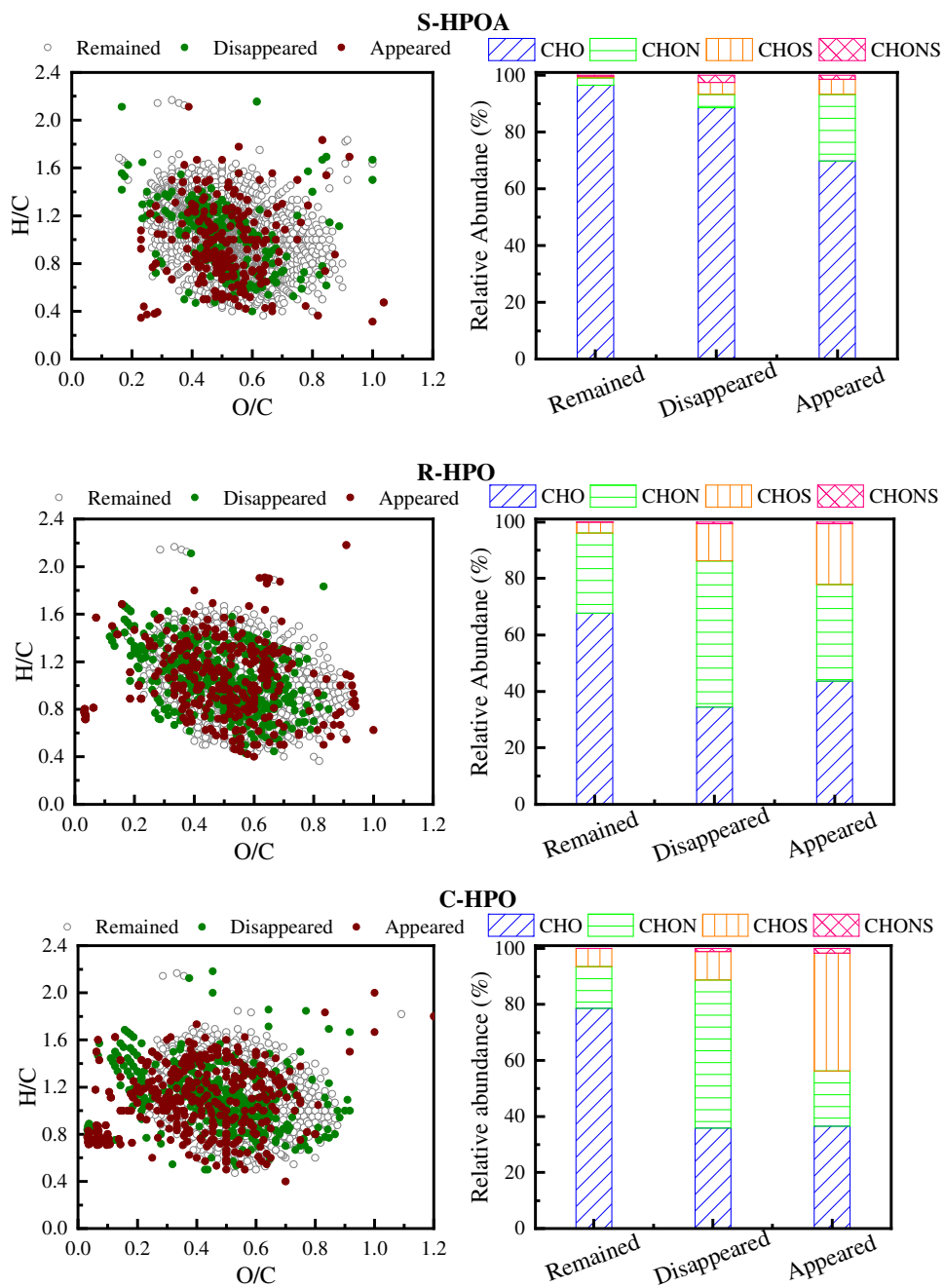


Fig. 3. van Krevelen diagrams (left) and relative abundance of molecules with different compositions (right) for the disappeared, remained and produced molecules upon 30 min UV irradiation.

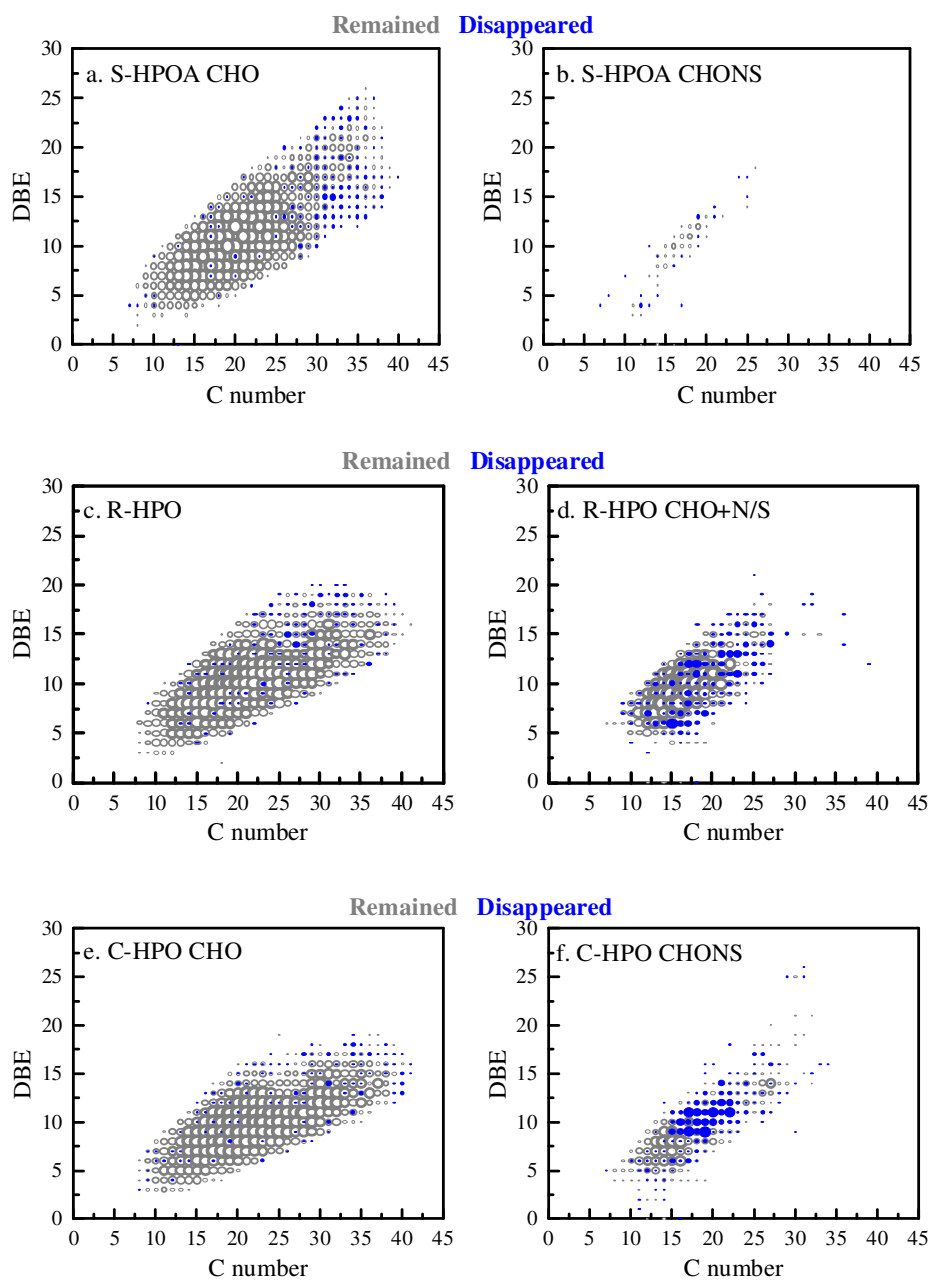


Fig. 4. DBE versus C number map showing distribution of disappeared and remained molecules containing (a,c,e) only CHO and (b,d,f) also N or S. Bubble size reflects the relative abundance of the molecules (i.e., the number of the molecules).

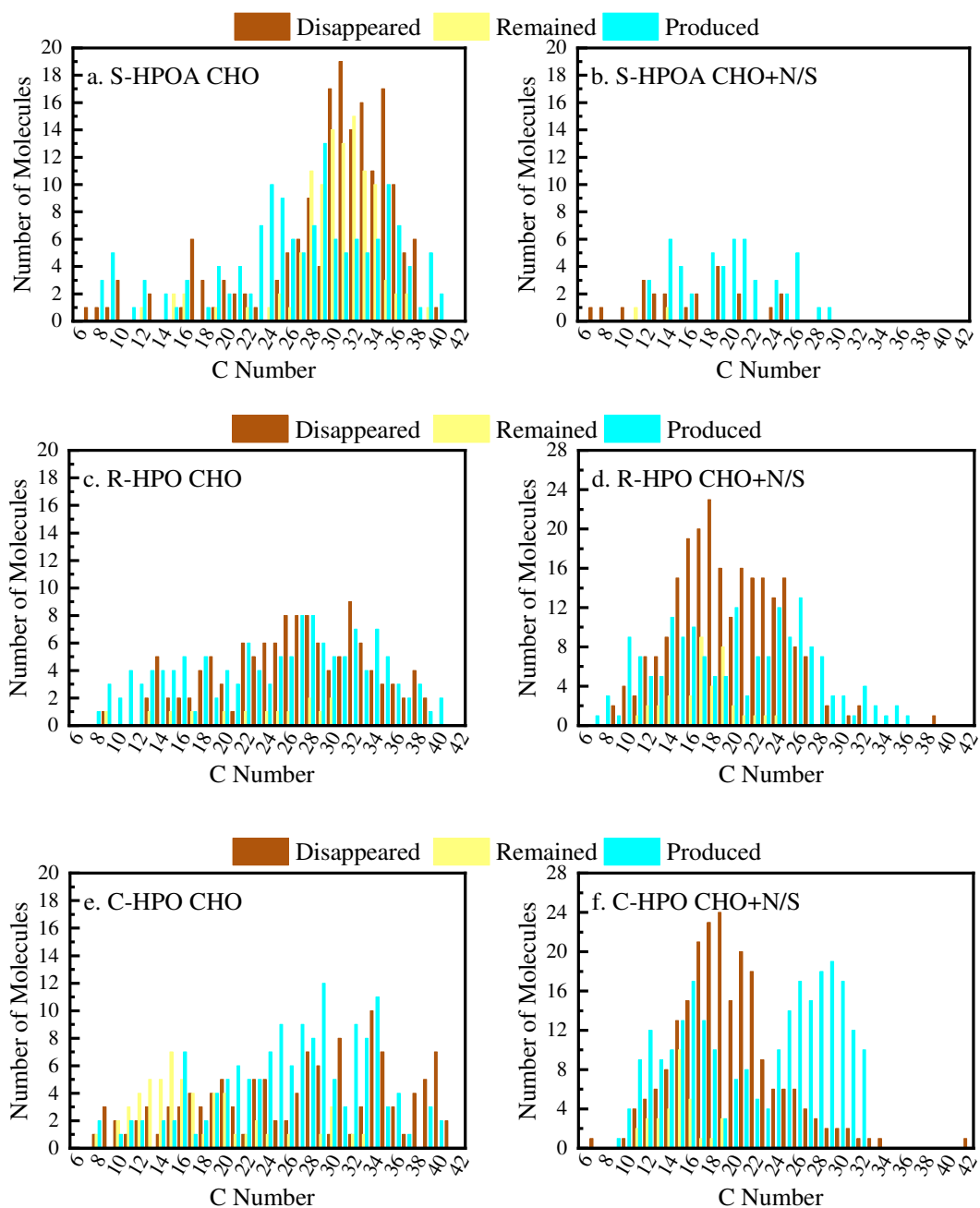


Fig. 5. Number of molecules associated with Carbon number within disappeared, remained and produced (a,c,e) CHO and (b,d,f) CHO+N/S community upon 30 min UV irradiation. Note: The remained molecules are only those with intensity decrease greater than 30%.

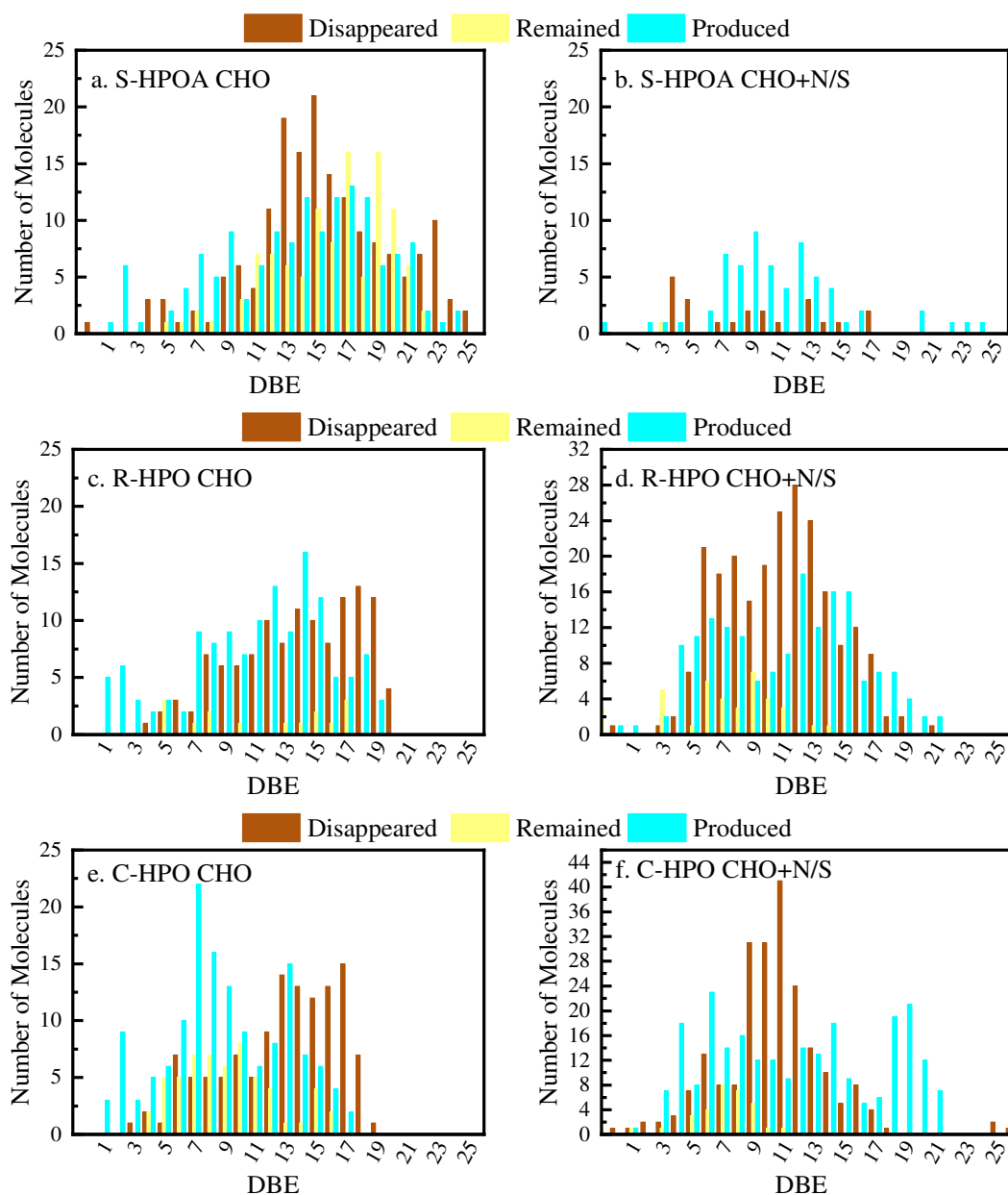
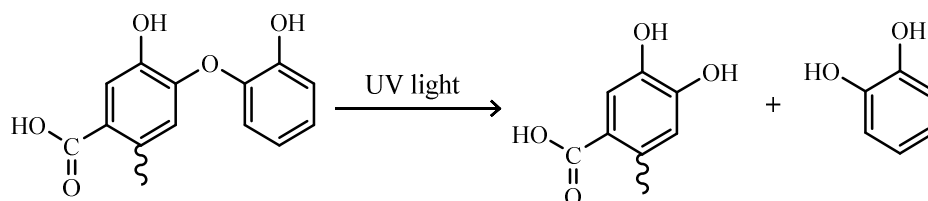
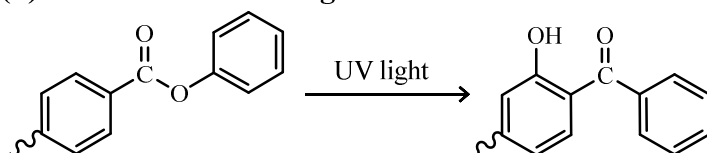


Fig. 6. Number of molecules associated with DBE within disappeared, remained and produced (a,c,e) CHO and (b,d,f) CHO+N/S community upon 30 min UV irradiation. Note: The remained molecules are only those with intensity decrease greater than 30%.

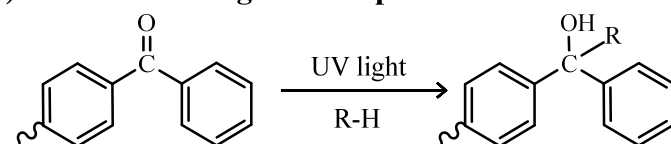
(a) Cleavage of linkages between aromatic structures



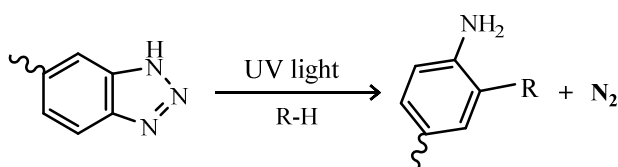
(b) Photo-Fries rearrangement



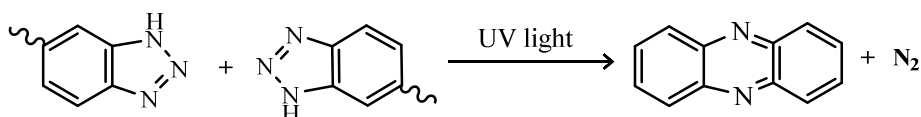
(c) Covalent linking of benzophenone



(d) Alkyl addition to benzotriazole structures



(e) Polymerisation of benzotriazole structures



Scheme 1. Representative illustrations on UV-induced reactions responsible for the observed DOM transformation. (a). Cleavage of large DOM molecules (b). Photo-Fries rearrangement of phenyl ester (c) Covalent linkages between benzophenone and target molecules. (d) Addition of alkyl to benzotriazole structures (e) Polymerization of benzotriazole structures. R-H represents active H-containing target molecules.

Table 1. Statistics and characteristics of molecules disappeared, remained, and appeared with 30 min exposure to UV.

| Sample | | Number (%) | Intensity (%) | H/C_{wa} | O/C_{wa} | m/z_{wa} | C_{wa} | DBE_{wa} | #CHO | #CHON | #CHOS | #CHONS |
|---------------|-------------|-------------------|----------------------|-------------------------|-------------------------|-------------------------|-----------------------|-------------------------|-------------|--------------|--------------|---------------|
| S-HPOA | disappeared | 192 (9.7) | 7.35E+08 (3.2) | 1.01 | 0.51 | 610.16 | 28.74 | 15.30 | 170 | 9 | 8 | 5 |
| | remained | 1782 (90.3) | 2.21E+10 (96.8) | 1.05 | 0.53 | 429.58 | 20.01 | 10.61 | 1719 | 47 | 9 | 7 |
| | appeared | 208 (10.5) | 8.06E+08 (3.5) | 0.93 | 0.50 | 535.88 | 25.47 | 14.76 | 145 | 49 | 11 | 3 |
| R-HPO | disappeared | 355 (12.3) | 1.59E+09 (4.1) | 1.06 | 0.49 | 486.18 | 22.50 | 11.94 | 122 | 184 | 47 | 2 |
| | remained | 2531 (87.7) | 3.74E+10 (95.9) | 1.12 | 0.53 | 422.09 | 19.48 | 9.63 | 1713 | 720 | 96 | 2 |
| | appeared | 307 (10.8) | 1.18E+09 (3.1) | 1.03 | 0.47 | 486.38 | 23.26 | 12.43 | 134 | 105 | 66 | 2 |
| C-HPO | disappeared | 340 (13.5) | 1.71E+09 (3.9) | 1.11 | 0.48 | 485.49 | 22.97 | 11.51 | 122 | 180 | 34 | 4 |
| | remained | 2173 (86.5) | 4.20E+10 (96.1) | 1.19 | 0.52 | 435.87 | 20.36 | 9.21 | 1709 | 322 | 141 | 1 |
| | appeared | 405 (15.7) | 2.34E+09 (5.3) | 0.98 | 0.30 | 465.18 | 25.32 | 14.22 | 148 | 80 | 170 | 7 |

Graphical Abstract

